

**Keywords:** absolute nodal coordinates; dynamic tire model; finite elements

**Dmitry POGORELOV\***, **Alexander RODIKOV**  
Bryansk State Technical University, Laboratory of Computational Mechanics  
bulv. 50 let Oktyabrya 7, Bryansk, 241035, Russia  
*\*Corresponding author.* E-mail: [pogorelov@universalmechanism.com](mailto:pogorelov@universalmechanism.com)

## THE TRAPEZOIDAL FINITE ELEMENT IN ABSOLUTE COORDINATES FOR DYNAMIC MODELING OF AUTOMOTIVE TIRE AND AIR SPRING BELLOWS. PART II: VERIFICATION

**Summary.** The second part of the paper includes numerical tests verifying equations of motion of flexible bodies in absolute coordinates with rectangle and isosceles trapezoid finite elements. The equations are formulated in the first part of the paper. The verification is based on three types of problems: calculation of natural frequencies and modes, evaluation of buckling, and computation of large static and dynamic deflections of flexible bodies. Tests show good agreement with the theoretical results and the results obtained by other authors.

### 1. INTRODUCTION

In the first part of the paper, we derived equations of motion of flexible bodies in absolute nodal coordinates [1]. A specific feature of the method used consists of application of the Craig–Bampton approach for deriving equations of motion of each of the finite elements in the body model. The practical implementation of the developed method in Universal Mechanism software is restricted at present by an isosceles trapezoid plate finite element. In this part of the paper, we verify the correctness and efficiency of the equations in respect to their use for simulation of uniform thin plates and shells, which, in particular, undergo large deflections.

The most frequently used method for verification of the dynamic equation of flexible bodies consists of computation of natural frequencies and modes for some benchmark problems. To verify the derived model, in Sect. 2, we consider two numerical tests for a flexible annular plate and a conical shell and compare the frequency values with the results obtained by other authors [2-3].

The ability of the equations to simulate large flexible deflections of bodies is tested in Sect. 3. Static tests with rectangle and annular plates under different distributed loads are compared with the known theoretical results as well as with the published analytical and numerical deflection values [4-6]. The final test corresponds to simulation of large dynamic oscillations of a rectangle plate with an attached rigid body; the simulation results are compared with the experimental data published in paper [7].

An example for the computation of a square plate buckling is considered in Sect. 4.

All computations in this paper are carried out taking into account linear stiffness matrix  $\mathbf{K}_0$  of the finite element (FE), neglecting the geometric stiffness matrix  $\mathbf{K}_\sigma$  and the stiffness matrix of large displacement  $\mathbf{K}_L$ .

## 2. NATURAL FREQUENCIES AND MODES

### 2.1. Annular plate

Consider an annular plate with free outer and inner edges. The plate geometrical parameters and material properties are as follows: inner radius  $R_i=0.16\text{m}$ , outer radius  $R_o=0.4\text{m}$ , thickness  $h=10\text{mm}$ , density  $\rho=7850\text{kg/m}^3$ , Young's modulus  $E=2.1\cdot 10^{11}\text{N/m}^2$ , and Poisson's ratio  $\nu=1/3$ .

Convergence of six lower natural frequencies computed according to equations of motion with an increase in the number of finite elements is presented in Tab. 1. The total number of finite elements is computed as the product of the number of elements in radial and transversal directions  $n_r \times n_\phi$ . The frequencies are compared for two variants of shape functions V1, V2 described in [1]. The last column in Tab. 1 presents the values of frequencies computed in paper [2] using the Hamiltonian approach. Analysis of the results shows that a good approximation of the lower frequencies can be obtained for a relatively small number of finite elements. The second variant V2 of the shape functions yields slightly better results than the first variant V1.

Table 1  
Convergence of lower natural frequencies of an annular plate (Hz) for different FE discretizations

	2×10		3×20		4×30		5×40		Zhou et al. [2]
	V1	V2	V1	V2	V1	V2	V1	V2	
$\omega_1$	76.48	75.52	73.18	72.36	72.83	71.81	72.79	71.62	71.02
$\omega_2$	134.86	137.67	134.19	135.31	134.35	134.93	134.46	134.81	134.00
$\omega_3$	204.90	200.90	192.08	190.05	190.13	187.65	189.61	186.72	184.35
$\omega_4$	284.99	274.90	276.96	268.08	277.07	267.71	277.76	267.82	267.06
$\omega_5$	377.00	369.61	350.99	346.99	345.36	341.13	343.66	338.72	333.17
$\omega_6$	507.88	509.73	515.91	495.45	345.36	494.05	511.60	493.79	491.34

The natural modes of free vibrations of the annulus are shown in Fig. 1.

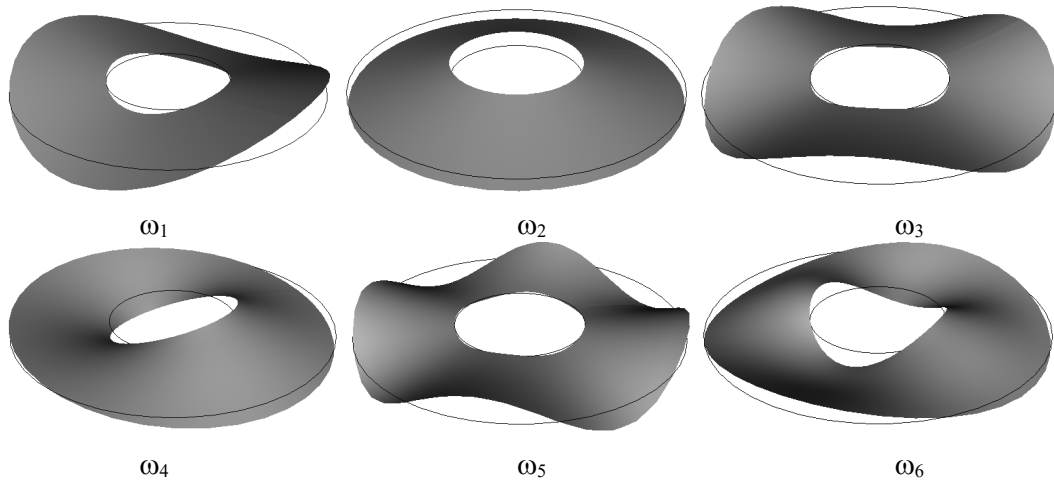


Fig. 1. Bending modes of an annular plate for six lower frequencies

### 2.2. Open conical panel

The second test verifies the ability of the element used in modeling shells. The test consists of computation of natural frequencies and modes for two conical panels with free edges described in paper [3]. The authors of this paper report both numerical and experimental values of frequencies. The panel geometrical parameters are shown in Fig. 2. Numerical values of the geometrical parameters and material properties for the panels are listed in Tab. 2.

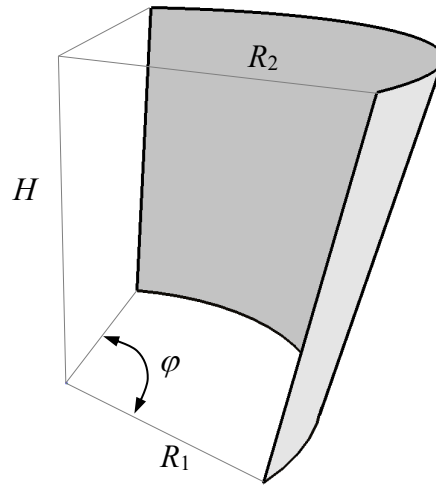


Fig. 2. Geometrical parameters of a conical panel

Table 2

Cone panel parameters

	$\varphi$ , deg	$R_1$ , m	$R_2$ , m	$H$ , m	$h$ , mm	$E$ , N/m <sup>2</sup>	$\rho$ , kg/m <sup>3</sup>	$\nu$
Cone 1	130	0.34	0.416	1.137	2	$0.7 \cdot 10^{11}$	2700	0.3
Cone 2	180	0.16	0.66	1.002	2	$0.7 \cdot 10^{11}$	2700	0.3

Table 3

Convergence of lower natural frequencies (Hz) for different FE discretizations, Cone 1

	5×5		10×10		20×20		Bardell et al. [3]	
	V1	V2	V1	V2	V1	V2	Computation	Experiment
$\omega_1$	7.81	7.36	7.75	7.26	7.59	7.07	7.21	7.5
$\omega_2$	12.86	12.84	12.66	12.62	12.50	12.46	12.32	12.7
$\omega_3$	19.13	18.6	19.11	18.58	19.01	18.45	18.21	18.2
$\omega_4$	35.93	35.78	35.53	35.41	35.37	35.23	34.40	35.6
$\omega_5$	45.81	44.85	46.05	45.62	45.92	45.45	44.32	46.0
$\omega_6$	51.45	49.36	70.08	69.88	69.76	69.47	67.78	59.5
$\omega_7$	52.43	50.12	79.62	77.74	78.69	77.32	75.43	70.4
$\omega_8$	69.90	65.05	80.36	78.48	79.44	77.96	76.05	73.1
$\omega_9$	72.55	67.11	90.97	90.59	90.73	90.25	87.80	90.4
$\omega_{10}$	77.38	68.42	117.55	117.31	116.74	116.56	113.65	N/A

Ten lower frequencies are computed with an increase in the number of elements  $n_r \times n_\varphi$  and are listed in Tabs. 3, 4 for two variants of shape functions V1, V2. The last two columns show the values of frequencies from paper [3]. Natural bending modes for the computed frequencies are shown in Fig. 3, 4. Similar to the previous test, a good correlation of the results is obtained.

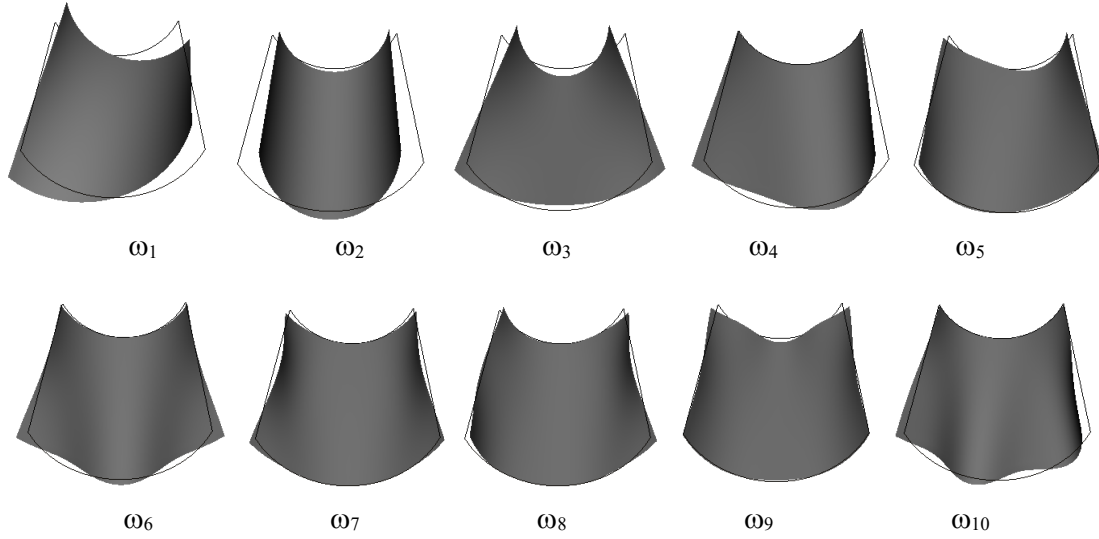


Fig. 3. Bending modes for Cone 1

Table 4  
Convergence of lower natural frequencies (Hz) for different FE discretizations, Cone 2

	5×5		10×10		20×20		Bardell et al. [3]	
	V1	V2	V1	V2	V1	V2	Computation	Experiment
$\omega_1$	4.44	4.40	4.39	4.34	4.37	4.31	4.65	4.5
$\omega_2$	9.00	8.52	8.95	8.48	8.86	8.34	8.75	8.9
$\omega_3$	11.00	10.82	11.60	11.36	11.56	11.28	11.32	11.5
$\omega_4$	18.14	17.78	20.95	20.84	20.83	20.69	20.85	20.9
$\omega_5$	21.70	21.46	22.25	21.72	22.41	21.77	22.63	21.7
$\omega_6$	27.27	26.39	33.22	32.93	33.16	32.94	33.06	33.2
$\omega_7$	33.60	31.97	46.42	45.99	47.33	46.95	47.83	46.6
$\omega_8$	36.20	35.27	47.18	46.42	47.81	47.32	47.87	47.4
$\omega_9$	45.93	40.76	61.77	60.28	63.88	63.37	63.51	58.6
$\omega_{10}$	46.24	44.64	63.48	62.21	68.76	67.64	67.95	63.7

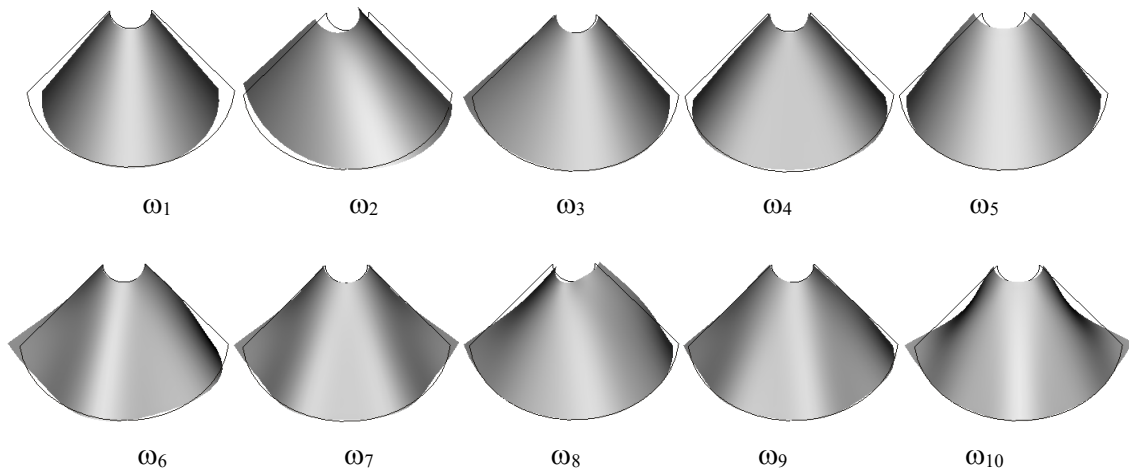


Fig. 4. Bending modes for Cone 2

### 3. LARGE STATIC AND DYNAMIC DEFLECTIONS OF PLATES

#### 3.1. Large deflection of a cantilever plate under a uniformly distributed load along a free edge

Consider a cantilever plate with clamped edge  $x=0$  and distributed load  $q$  along the free edge  $x=a$ . The load  $q$  is set in such a way that the plate has large deflections. The geometrical parameters and material properties of the plate are as follows: length  $a=0.5\text{m}$ , width  $b=0.2\text{m}$ , thickness  $h=5\text{mm}$ , Young's modulus  $E=2.1 \cdot 10^{11}\text{N/m}^2$ , and Poisson's ratio  $\nu=0.25$ .

In this example and in other static tests described below, large deflections of the plates are computed by integration of the equations of motion with increased dissipation. Thus, the oscillation amplitude decreases much faster than in the real cases, but the final solution when the oscillations have ceased corresponds to the solution of the static large deflection equations with good accuracy, Fig. 5.

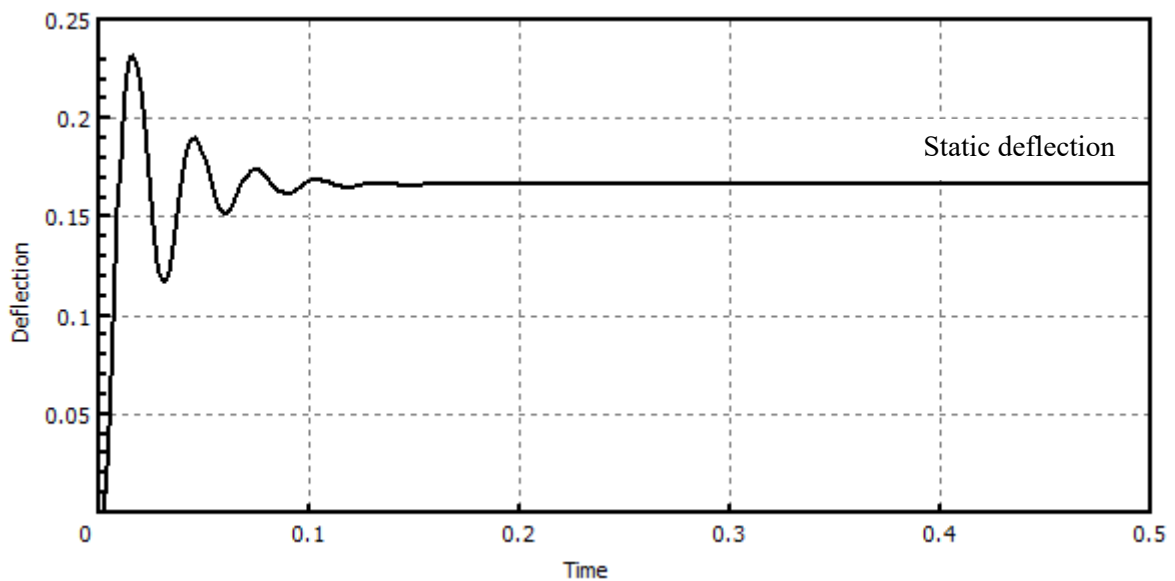


Fig. 5. Determination of static deflection using the time-integration method

Dimensionless horizontal and vertical deflections of the loaded edge for different load ratios  $qa^2/D$  and FE discretization of the plate  $n_l \times n_t$  in longitudinal and transversal directions are presented in Tab. 5. The last column shows the values of deflection computed in [4] using the theory of large deflection of beams. Deflected shapes of the plate in the  $xz$  plane are shown in Fig. 6. The results presented show that even a coarse FE discretization shows good agreement with the exact deflection values so that the maximal relative error is less than 1%.

Table 5

Large deflections of a cantilever plate

$qa^2/D$	3x1		5x5		Nonlinear beam theory [4]	
	$u/a$	$w/a$	$u/a$	$w/a$	$u/L$	$w/L$
0.25	0.004	0.085	0.004	0.085	0.004	0.083
0.50	0.017	0.167	0.016	0.165	0.016	0.162
0.75	0.036	0.243	0.035	0.239	0.034	0.235
1	0.060	0.310	0.057	0.305	0.056	0.302
2	0.168	0.502	0.162	0.497	0.160	0.494
3	0.263	0.610	0.255	0.606	0.255	0.603
4	0.337	0.676	0.329	0.673	0.329	0.670
5	0.396	0.718	0.388	0.717	0.388	0.714
6	0.442	0.748	0.435	0.748	0.434	0.744
7	0.479	0.771	0.473	0.771	0.472	0.767
8	0.511	0.788	0.505	0.788	0.504	0.785
9	0.537	0.802	0.532	0.803	0.531	0.799
10	0.560	0.814	0.555	0.815	0.555	0.811

### 3.2. Large deflections of a square plate with clamped edges under uniform normal pressure

Consider a square plate with clamped edges under uniform normal pressure  $p$  producing large deflections. The geometrical parameters and material properties of the plate are as follows: length of side  $a=2\text{m}$ , thickness  $h=5\text{mm}$ , Young's modulus  $E=2.1 \cdot 10^{11}\text{N/m}^2$ , and Poisson's ratio  $\nu=0.316$ .

Dimensionless deflections of the center of the plate for different pressure ratios  $pa^4/Eh^4$  and FE discretization of the plate are presented in Tab. 6 and shown in Fig 7. The last column in Tab. 6 shows the values of deflections computed in [5] using the von Karman large-deflection equations. Deflections of the plate's central section, which is parallel to the plate edge, for different pressure ratios are shown in Fig. 8. Analysis of the results shows that on refining FE discretization, a convergence to the exact solution is observed.

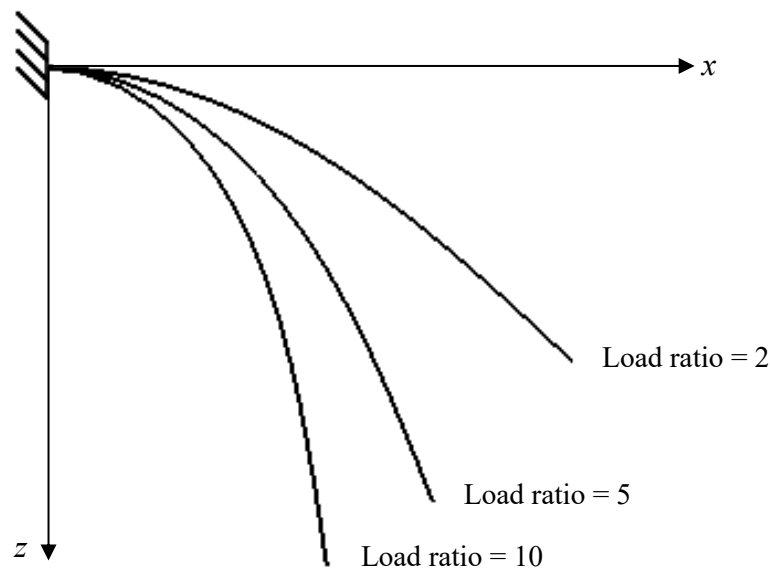
Fig. 6. Deflected shapes of a plate in the  $xz$  plane

Table 6

Dimensionless ( $w/h$ ) deflections of the center of the clamped plate

$pa^4 / Eh^4$	4x4	8x8	16x16	Levy's solution [5]
17.79	0.264	0.244	0.238	0.237
38.3	0.530	0.486	0.474	0.471
63.4	0.789	0.718	0.699	0.695
96.0	1.047	0.947	0.920	0.912
134.0	1.282	1.156	1.122	1.121
184.0	1.512	1.361	1.320	1.323
245.0	1.737	1.564	1.516	1.521
318.0	1.953	1.760	1.706	1.714
402.0	2.158	1.946	1.887	1.902

### 3.3. Large deflection of an annular plate loaded in the center with a concentrated force

Consider an annular plate undergoing large deflection. A rigid body is attached to the inner edge of the plate, which is loaded in the center with the concentrated force  $P$ , Fig. 9. The outer edge of the plate is clamped. The geometrical parameters and material properties of the plate are as follows: inner radius  $R_i=0.5\text{m}$ , outer radius  $R_o=2\text{m}$ , thickness  $h=5\text{mm}$ , Young's modulus  $E=2.1 \cdot 10^{11}\text{N/m}^2$ , and Poisson's ratio  $\nu=0.25$ .

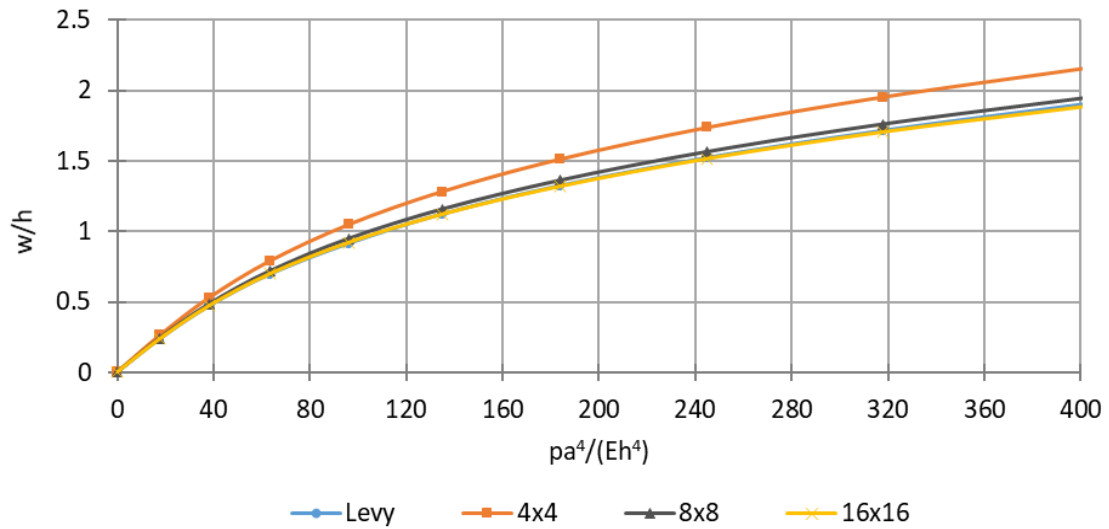


Fig. 7. Dimensionless ( $w/h$ ) deflections of the center of the clamped plate

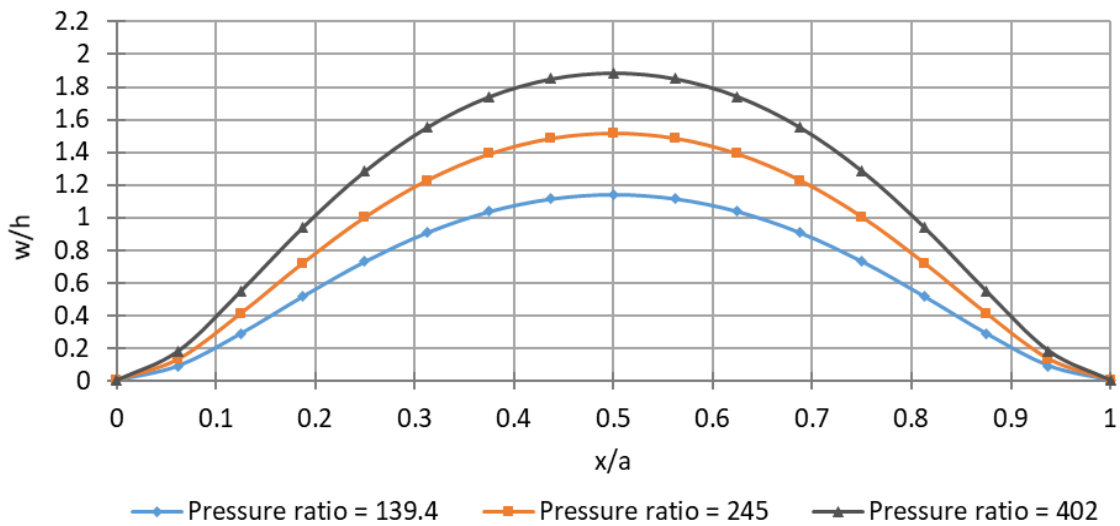


Fig. 8. Dimensionless deflections of the plate section

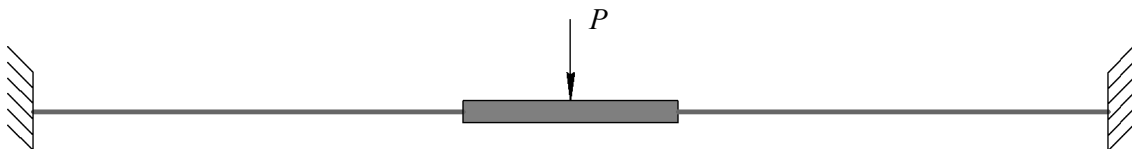


Fig. 9. Annular plate with an attached rigid body in the hole

Dimensionless deflections of the free edge of the plate for different force ratios  $PR_o^4 / Eh^4$  and FE discretization of the plate in radial and transversal directions  $n_r \times n_\varphi$  are presented in Tab. 7. The last column in Tab.7 shows the values of deflections computed in [6] by the numerical solution of von Karman equations using the collocation method. Deflections of the plate's radial section for different load ratios are shown in Fig. 10. This test confirms the applicability of the trapezoid element for the analysis of large deflections of thin plate structures.

Table 7

Dimensionless ( $w/h$ ) deflections of the free edge of the annular plate

$PR_o^4 / Eh^4$	4x16	8x16	16x16	Dumir et al. [6]
10	0.7167	0.7048	0.7013	0.7016
20	1.1020	1.0819	1.0760	1.0778
30	1.3659	1.3405	1.3327	1.3408
40	1.5719	1.5425	1.5334	1.5332
50	1.7435	1.7111	1.7008	1.7052

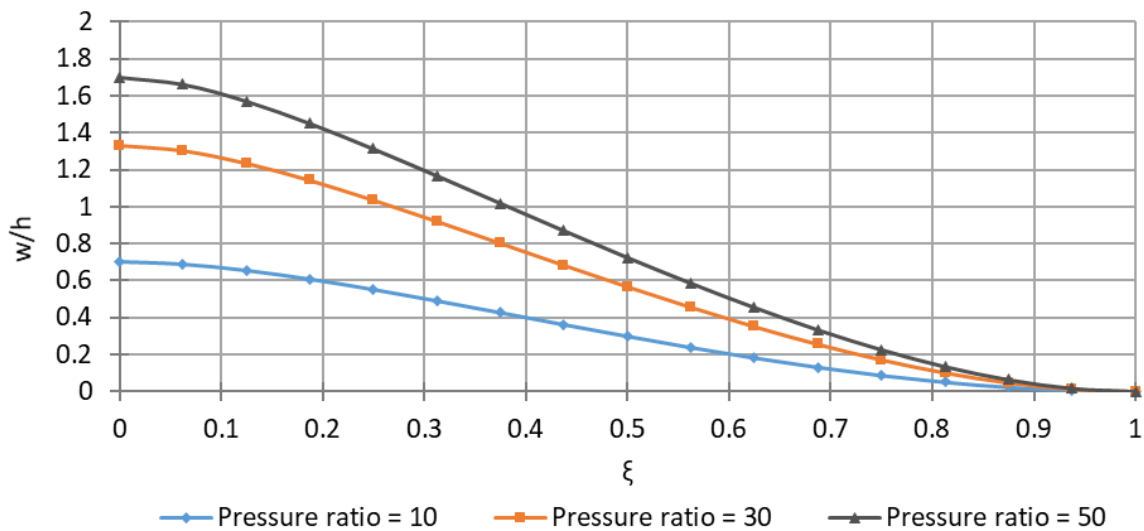


Fig. 10. Dimensionless deflections of a plate's radial section

### 3.4. Large oscillations of a rectangular thin plate with an attached rigid body

Consider a dynamic simulation of a plate according to the experiment described in paper [7], Fig. 11. A rectangular plate 10×40cm in size is clamped on a short edge and loaded by a weight of the attached body in a vertex opposite to the clamping edge. During the experiment, the plate falls freely from the horizontal position. Large plate oscillations are recorded by cameras, and Cartesian coordinates are extracted for the attachment point of the body. The thickness of the plate is 0.5 mm, Young's modulus  $E=1.89 \cdot 10^{11} \text{N/m}^2$ , and Poisson's ratio  $\nu=0.3$ . The mass of the attached body is 0.26kg.

A comparison of the numerical simulation for the plate oscillations with the experimental results is shown in Fig. 12. The plate model contains 8×20 finite elements, and the attached body is considered a rigid one. The curves correspond to the lateral (X), longitudinal (Y), and vertical (Z) displacements of the attachment point. Fig 13 shows the convergence of simulation results with an increase in the number of elements in the model.

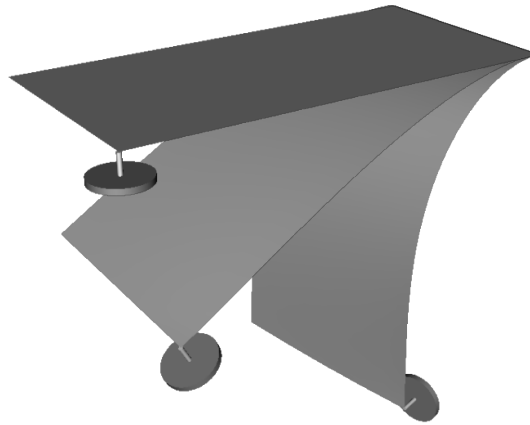


Fig. 11. Large dynamic oscillations of a plate

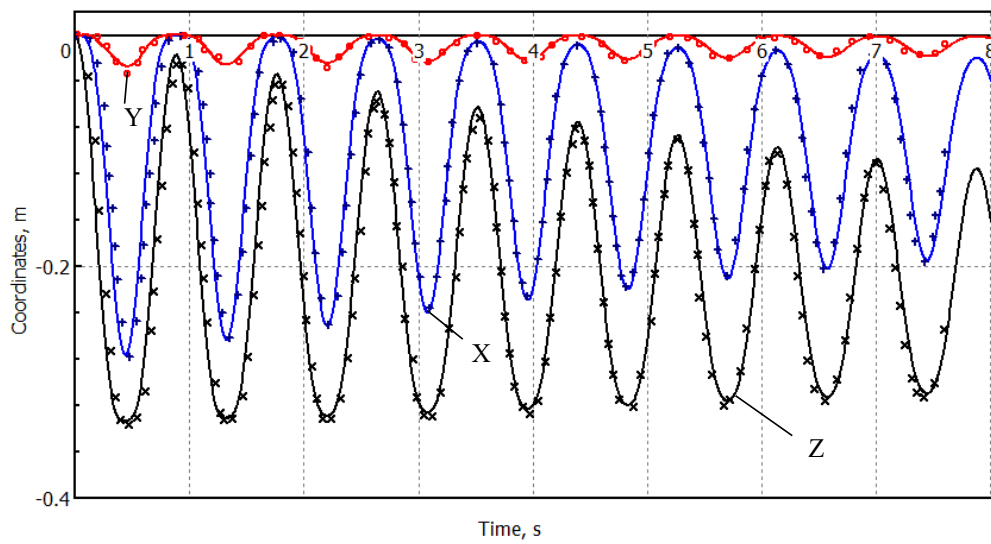


Fig. 12. Comparison of simulation (solid lines) and experimental (markers) results

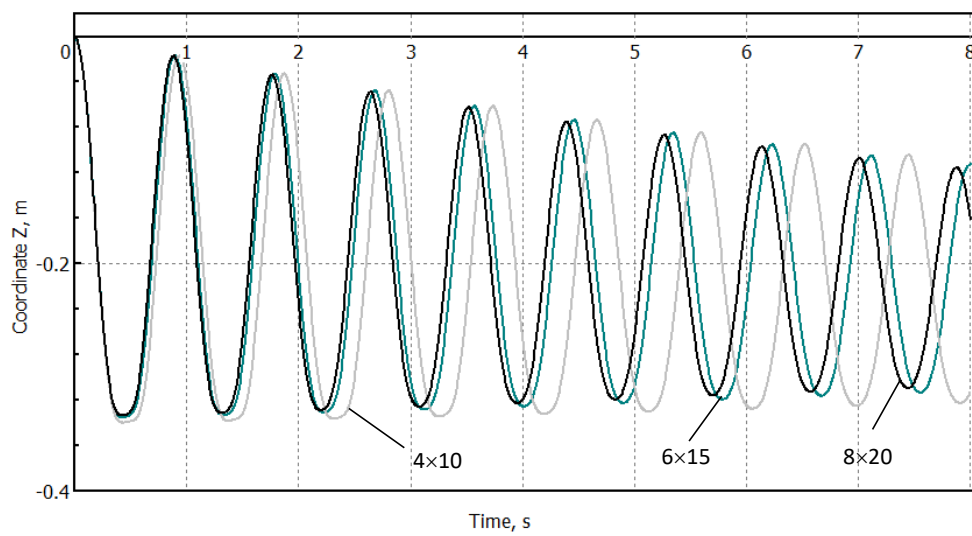


Fig. 13. Comparison of simulation results of plate oscillations for different plate meshings

#### 4. BUCKLING OF A SIMPLY SUPPORTED SQUARE PLATE

Consider a square plate with simply supported edges under compressive loading in-plane of the plate in the  $x$ -direction. The geometrical parameters and material properties of the plate are as follows: length of side  $a=2\text{m}$ , thickness  $h=5\text{mm}$ , Young's modulus  $E=2.1 \cdot 10^{11}\text{N/m}^2$ , and Poisson's ratio  $\nu=0.25$ .

In this test, the "natural frequency–compressive load" relationship is plotted. It is known that when a plate is compressed, its natural frequencies decrease. When the compressive load is critical, buckling occurs and the lowest natural frequency becomes zero.

The "lowest natural frequency–compressive load" relationships for 4x4, 5x4, and 6x6 FE meshes are shown in Fig. 14. In the figure,  $\omega/\omega_0$  is the dimensionless frequency,  $\omega_0$  is the theoretical value of the lowest natural frequency of the simply supported uncompressed plate,  $q/q_{cr}$  is the dimensionless load, and  $q_{cr} = 4\pi^2 D/b^2$  is the theoretical value of the critical load for the simply supported plate. Values of the dimensionless critical load approximation are 1.086 for a 4x4 mesh, 1.050 for a 5x5 mesh, and 1.019 for a 6x6 mesh.

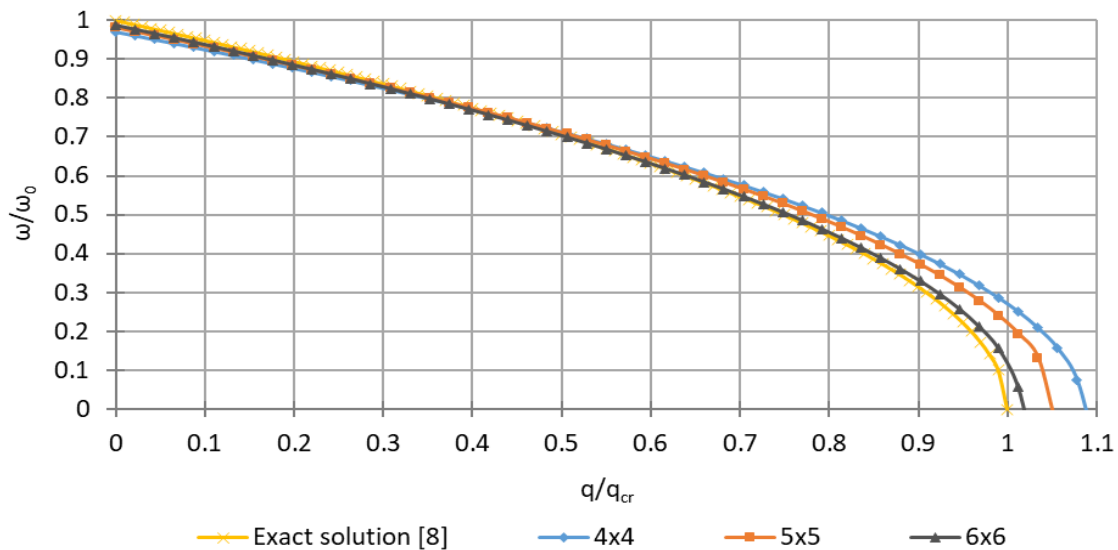


Fig. 14. "Lowest natural frequency–compressive load" relationships for different FE discretizations

#### 5. CONCLUSION

Computation of natural frequencies in Sect. 2 and comparison of their values with the results of other authors show that the derived equations of motion of flexible plates and shells yield quite an exact approximation of lower frequencies of flexible bodies.

The ability of the derived equation of motion in absolute coordinates to simulate large deflections of thin flexible bodies in solving both static and dynamic problems is confirmed in Sect. 3. It is important that equations of motion for separate finite elements are generated taking into account the linear stiffness matrix  $\mathbf{K}_0$  of FE. Nevertheless, the solutions of large deflection problems converge practically to exact ones with an increase in the number of finite elements, and this fact is the principal property of the absolute nodal coordinates. It is clear that the use of additional terms of the FE stiffness matrix corresponding to the nonlinear terms can improve the convergence, and we intend to continue the research in this direction.

An example in Sect. 4 shows that the derived equations of motion are able to predict the buckling of thin plates correctly without taking into account the geometric stiffness matrix  $\mathbf{K}_\sigma$  of FE.

## Acknowledgments

This research was supported by the Russian Foundation for Basic Research under grant 18-41-320004.

## References

1. Pogorelov, D.Y. & Rodikov, A.N. The trapezoidal finite element in absolute coordinates for dynamic modeling of automotive tire and air spring bellows. Part 1: Equations of motion. *Transport Problems*. 2021. Vol. 16. No. 2. P. P. 141-152.
2. Zhou, Z.H. & Wong, K.W. & Xu, X.S. & et al. Natural vibration of circular and annular thin plates by Hamiltonian approach. *Journal of Sound and Vibration*. 2011. No. 330. P. 1005-1017.
3. Bardell, N.S. & Dunsdon, J.M. & Langley, R.S. Free vibration of thin, isotropic, open conical panels. *Journal of Sound and Vibration*. 1998. No. 217. P. 297-320.
4. Gere, J.M. & Timoshenko, S.P. *Mechanics of Materials*. 3rd Edition. Springer US. 1991. 827 p.
5. Levy, S. *Square plate with clamped edges under normal pressure producing large deflections*. Report No. 740. Washington, D.C.: National Advisory Committee for Aeronautics. 1941. 14 p.
6. Dumir, P.C. & Nath, Y. & Gandhi, M.L. Non-linear axisymmetric static analysis of orthotropic thin annular plates. *International Journal of Non-Linear Mechanics*. 1984. Vol. 19(3). P. 255-272.
7. Yoo, W.S. & Lee, J.H. & Park S.J. & et al. Large deflection analysis of a thin plate: Computer Simulations and Experiments. *Multibody System Dynamics*. 2004. Vol. 11. P. 185-208.
8. Биргер, И.А & Пановко, Я.Г. *Прочность, устойчивость, колебания. Справочник в трех томах*. Том 3. Москва: Машиностроение. 1968. 570 с. [In Russian: *Strength, stability, vibrations. Handbook in three volumes*. Vol. 3].

Received 17.10.2019; accepted in revised form 07.09.2021